Sensitive *Leptospira* DNA Detection using Tapered Optical Fiber Sensor

N. H. Zainuddin[1,2], H.Y. Chee[3], M.Z. Ahmad[4], M. A. Mahdi[1,2], M. H. Abu Bakar[1,2], M. H. Yaacob[1,2]

[1]Department of Computer and Communication Systems, Faculty of Engineering, Universiti Putra Malaysia, 43400 UPM Serdang, Selangor, Malaysia.

[2]Wireless and Photonic Networks Research Centre (WiPNET), Universiti Putra Malaysia, 43400 UPM Serdang, Selangor, Malaysia.

[3]Department of Microbiology and Parasitology, Faculty of Medicine and Health Sciences, Universiti Putra Malaysia, 43400 UPM Serdang, Selangor, Malaysia.

[4]Biotechnology and Nanotechnology Research Center, Malaysian Agricultural Research and Development Institute (MARDI), 43400 Serdang, Selangor, Malaysia.

Email: hanif@upm.edu.my

Abstract:

This paper presents the development of tapered optical fiber sensor to detect a specific *Leptospira* bacteria DNA. The bacteria causes *Leptospirosis*, a deadly disease but with common early flu-like symptoms. Optical single mode fiber (SMF) of 125 µm diameter is tapered to produce 12 µm waist diameter and 15 cm length. The novel DNA-based optical fiber sensor is functionalised by incubating the tapered region with sodium hydroxide (NaOH), (3-Aminopropyl) triethoxysilane (APTES) and glutaraldehyde. Probe DNA is immobilized onto the tapered region and subsequently hybridized by its complementary DNA. The transmission spectra of the DNA-based optical fiber sensor is measured in the 1500 - 1600 nm wavelength range. It is discovered that the shift of the wavelength in the SMF sensor is linearly proportional with the increase in the complementary DNA concentrations from 0.1 nM to 1.0 nM. The sensitivity of the sensor towards DNA is measured to be 1.2862 nm/nM and able to detect as low as 0.1 fM. The sensor indicates high specificity when only minimal shift is detected for non-complementary DNA testing. The developed sensor is able to distinguish between actual DNA of *Leptospira* serovars (Canicola and Copenhageni) against Clostridium difficile (control sample) at very low (femtomolar) target concentrations.

Keywords: *Leptospira* bacteria; leptospirosis disease; tapered optical fiber; DNA biosensor; wavelength shift; infrared detection; femtomolar concentrations;

This article has been accepted for publication and undergone full peer review but has not been through the copyediting, typesetting, pagination and proofreading process, which may lead to differences between this version and the Version of Record. Please cite this article as doi: 10.1002/jbio.201700363

1. Introduction

Thin, helically coiled and motile spirochetes *Leptospira* is a water borne bacterium that causes leptospirosis disease to human [1]. Human patients infected by *Leptospira* bacteria exhibit sudden onset of fever, chills, and headache [2]. In both mild and severe forms of leptospirosis, flu-like symptoms develop first. However, these signs and symptoms are nonspecific which may be indistinguishable with other diseases such as influenza, dengue or malaria[2-3]. The vague clinical signs make leptospirosis likely to be under-diagnosed, leading to delayed treatment. Without early treatment, the patient may enter a more severe stage, which could lead to kidney failure, meningitis, liver failure, respiratory distress, and even death [2, 4]. In one clinical study in Malaysia, the pervasiveness of leptospirosis surged from year 2004 to 2009 with the Ministry of Health Malaysia (MOH) reported an increase in number of cases from 263 to 1418. The number of deaths due to the disease is recorded at 193 with fatality rate varying from 1.8% to 7.6% for the 5-years period [5-6]. In view of the fact that leptospirosis disease is spreading ruthlessly, the importance of a highly efficient *Leptospira* DNA detection system is at the utmost priority.

Currently, culture and microscopic agglutination test (MAT) are gold standard methods for leptospirosis diagnosis [7]. However, these methods are inadequate for early diagnosis. In the case of *Leptospira* culture, the colonies are slow-growing bacteria and for MAT, the anti-*Leptospira* antibodies can only be detected by the second week after onset of symptoms. MAT is also limited by its subjectivity, and require the maintenance of live *Leptospira* as well [8]. Therefore, an efficient laboratory diagnostic system on leptospirosis is required to eliminate clinical suspicion at the early acute phase of the disease. The presence of the *Leptospira* in the blood increases exponentially from day 0 to day 7 occurring in parallel with the onset of the symptoms [9]. Therefore, the existing effort for early leptospirosis diagnosis is directed towards the detection of *Leptospira* bacteria, its antigen or DNA. Out of these three, DNA is the intracellular property that is commonly investigated for high specificity detection [10–12]. In contrast, the extracellular properties of *Leptospira* bacteria or its antigen tend to lose their specific binding activity due to the fact that the conformation for most of the protein might probably be denatured after being removed from their natural environment [13, 14]. Besides that, DNA-based detection can be performed in either live or dead cells and does not require microorganism isolation [15, 16].

The key mechanism in the DNA-based detection is the binding between the single-stranded DNA (or probe) immobilized onto a surface of transducing platform with specific single-stranded DNA sequence (or target). This binding event produces a measurable signal

that can be used as the detection parameter [17]. Common transducing platform for the biosensor system is electrical-based such as conductometric. Electrical-based biosensor system is low cost and sensitive. However, this conventional detection system is known to be prone to electromagnetic interference as well as poor specificity. The utilization of optical fiber becomes an alternative application in the biotechnology and molecular biology realm. The significant advantages of optical fiber technology such as compact size, light weight and electromagnetic interference immunity create strong interest towards biosensor based on optical fiber [18-19]. Its abilities to operate *in situ*, reduced setup dimension, minimal invasion for *in vivo* measurement while providing high sensitivity and specificity make the optical fiber biosensor an exciting prospect compared to the conventional electrical counterpart [19-20].

An interesting method to improve the sensing performance in optical fiber sensor is by modifying the physical of the transducing platform. One of the most reliable optical fiber platform modification methods is tapering. The tapering process 'shrinks' the optical fiber core and cladding and thus, changing the light propagation in the tapered optical fiber [21]. As a result, the evanescent field interaction around the optical fiber is enhanced [22]. The transducing platform becomes highly sensitive to any changes of refractive index near to its surface. When the tapered region is functionalised with a sensing layer, any reaction with the sample of interest will change the sensing layer properties and the evanescent field. Therefore, the detected light propagating in the tapered optical fiber is proportionally changed according to the sample concentrations [23]. Some of the well-established works on tapered optical fiber were reported by Brambilla and Wang et al [24, 25]. In general, these works focus on the modification of single mode fiber via tapering as well as its sensing applications for physical parameters such as humidity and temperature. The advantages of optical fiber tapering for various sensing applications in physical, chemical and biomolecule detection have been presented in [24-34].

Tapering offers simpler and more controlled modification than other fiber fabrication techniques such as grating. The fiber modification via grating requires extra processes such as bending, polishing and chemical etching. In contrast, fiber tapering only involves heating and pulling which is highly controllable with the use of glass processing workstation. Some studies have also reported higher sensitivity achievement in refractive index based sensing for the optical fiber modified via tapering. For example, the tapering-based sensor in [37] and [38] produced sensitivity around 1500 nm/RIU and 19212.5 nm/RIU, respectively, as

compared to the gratings-based sensors in [35] and [36] with 1.1nm/RIU and 660 nm/RIU, respectively.

In case of biosensor and DNA detection, some development using gratings-based optical sensors have been reported. Bertucci et al. [6] utilised PNA-based microstructure optical fiber (MOF) Bragg gratings to detect unamplified genomic DNA. High performance is reported with minimal concentration detected of 0.3 ng/ml at very low sample volume (10 μL). The developed sensor used gold nanoparticle as a catalyst. Another interesting and advanced Bragg gratings based sensors is presented by Candiani et al. [39] for label free DNA detection. Double tilted fiber Bragg gratings are employed to create modified Fabry-Perot core-cladding closed-loop cavity. This approach is demonstrated to be independent from external interferences such strain and temperature. The sensing performances also show high specificity with mismatch DNA strands at 100 nM and 10 nM concentrations. Both studies indicate an opportunity for sensing improvement using taper-based optical fibers which are able to detect DNA and protein at lower concentrations than 10 nM without any gold catalyst [40-42].

Resonator is also another optical device commonly used for biosensing applications by exploiting the surrounding refractive index. Some published works [43] and [44] have reported on the optimization of whispering gallery resonator to achieve high sensing performance via refractive index change. Franchois et al, successfully optimised refractive index change in 10 μm dye doped polystyrene microsphere resonator upon lasing excitation (FWHM ~80 pm at 600 nm and produced sensitivity of 50 nm/RIU [44]. However, alternative excitation scheme have to be optimised if the resonator size is reduced below 10 μm because the value is too close to the lasing threshold damage. The sensitivity optimisation is less complicated for tapering based modification. The sensitivity achieved in tapered fiber is also typically much higher in the range of 1000 – 1900 nm/RIU with smaller taper dimension.

In this work, a leptospirosis biosensor system utilizing a tapered and functionalised optical fiber is developed to detect *Leptospira* DNA sequence. The *Leptospira* capture probe DNA was uniquely designed and aligned based on rrs gene of *Leptospira* spp. Therefore, this novel optical fiber based biosensor produces different wavelength shifts upon exposure to solely *Leptospira* DNA with several concentrations. The developed biosensor also shows high sensitivity and specificity towards different actual *Leptospira* bacteria DNA samples. The findings here are noteworthy as well as providing new insights in leptospirosis diagnostic.

2. Experimental

2.1 Fabrication and characterization of tapered optical fiber

The tapered optical fiber is fabricated using glass processor workstation (Vytran GPX-3400). The machine modifies the optical fiber dimension by pulling the two ends of the optical fiber while it is heated by a unique filament. The real-time control system allows a customised dimension, uniformity and reproducibility of the fabricated taper by controlling the pulling speed and heat at a constant value of 1 mm/s and 42 W, respectively. As displayed in Figure 1, the tapered section is created at the center of 1 m step index single-mode optical fiber (Lucent Allwave Fibre) with symmetric up and down taper transition lengths of 5 mm. The optical fiber initial cladding diameter of 125 µm is tapered down to 12 µm and the tapered waist length is fixed at 15 mm. These dimensions have been optimized for ligand-target protein interaction as reported in the previous work [45]. The featured dimensions are validated under the machine's CCD camera and examined using the optical microscope (Motic BA210).

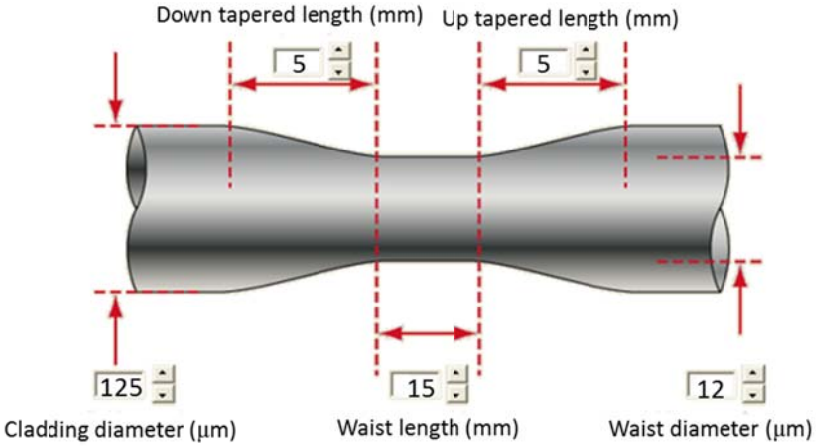

Figure 1 Schematic diagram of single mode optical fiber tapered profile.

The optical properties of the tapered optical fiber are characterised by comparing its sensitivity using sodium chloride (NaCl) solution. The 1 M of 10 ml NaCl (Sigma-Aldrich) solution is diluted with deionized water (DI water) to desired concentrations for the characterisation testing. In this study, several NaCl concentrations (0.2 M, 0.4 M, 0.6 M, and 0.8 M) with different refractive indices (RI) are employed. Prior characterisation testing, the RI of each NaCl concentration is measured by using handheld optical refractrometer (ATAGO B028977).

2.2 Functionalisation of tapered optical fiber

The functionalisation process is crucial to promote conjugation between inorganic materials like the tapered optical fiber surface with organic biomolecules. This process is the first step in the biosensor preparation to hybridize the *Leptospira* DNA onto the transducing platform. The functionalization of the tapered optical fiber region is performed through covalent modification using bi-functional linkers [46]. In this process, the chemicals/linkers involved are sodium hydroxide (NaOH), 3-aminopropyltriethoxysilane (APTES), and glutaraldehyde (Sigma-Aldrich). The function of NaOH is to improve the attachment of APTES with the fiber surface by enriching the hydroxyl groups (-OH) on the surface. The use of NaOH is well-established in biosensor as reported in some previous works [47, 48]. APTES is a silanization reagent and highly important to convert hydroxyl group into amine group so that the surface is susceptible for the bonding with the aldehyde group [46]. Finally, glutaraldehyde as a bifunctional aldehyde is deposited onto the fiber surface to form an arm linker, which makes it possible for probe DNA to be covalently bonded with fiber surface [49]. This technique has been successfully demonstrated in several studies [50-54].

Figure 2 summarises the process to functionalise the tapered optical fiber surface. At first, the tapered optical fiber region is treated with 0.1 M NaOH for duration of 45 minutes. After the duration to generate –OH, the tapered optical fiber region is silanized with APTES for 45 minutes to obtain the amine-modified surface. Subsequently, the tapered optical fiber region is cross-linked with glutaraldehyde for 1 hour. Both concentrated APTES (98%) and glutaraldehyde (50%) are diluted to meet 2% v/v in deionized water which equivalent to 0.09 M and 0.43 M solutions, respectively. The concentrations of the mixed solutions are specified based on the previous studies [55–57] in order to get stable covalent bonding layer on the solid surface [49].

After each chemical treatment, the tapered optical fiber region is rinsed with deionized water (three times) and air-dried. The morphologies of the linkers on the fiber surface are characterised and observed by Hitachi S-3400N Scanning Electron Microscopy (SEM) and their transmission output spectra are recorded via optical spectrum analyser (Yokogawa AQ6331).

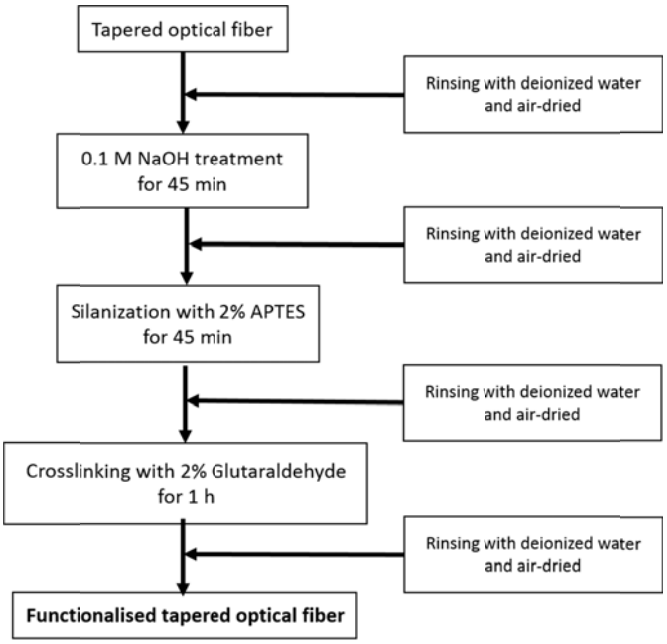

Figure 2 Tapered optical fiber functionalization process.

2.3 *Leptospira* DNA immobilization and hybridization

At this point, the aldehyde-functionalised tapered optical fiber is available to be bonded with the probe DNA. DNA detection can be achieved when a target DNA strand creates a tethered nucleotide via hybridization process with the single-stranded probe DNA [33]. Therefore, in this work, several synthetic single-stranded DNAs (Integrated DNA Technologies) were employed. All the desired DNA concentrations are diluted using sterile ultrapure water. The probe sequences adduced from [58] with their respective designed sequences targeting 16S ribosomal RNA (rrs) gene are tabulated in Table 1 as well as with their non-complementary sequence. In this work, non-complementary sequence that exhibits large difference in order than the right complementary sequence is preferred as a control sample. Sequence variability of 4 to 5 nucleotide bases occurs in the targeted gene from different pathogenic *Leptospira*. Therefore, single-base mismatch oligonucleotide is not suitable to be used as a negative control in this case because probe DNA is expected to bind to these sequences (even with single-base mismatch) when it is used to test on various serovars or strains of *Leptospira* DNA. Several studies in DNA biosensor also show the specificity testing relies on large mismatched sequence towards probe sequence [59–61]. Therefore, this non-complementary sequence used as a control sample in this work is appropriate for specificity test.

Table 1 List of oligonucleotide sequences.

Type of synthetic DNA	Sequence of DNA
Probe	5'-CTT CGG ATT GTA AAG TTC ADT-3'
Complementary	5'-AHT GAA CTT TAC AAT CCG AAG-3'
Non-complementary	5'-AGA GCG CAA TGC CAT AAG TAC-3'

Figure 3 summarises the process of hybridizing the target DNA onto the tapered optical fiber surface. The aldehyde-functionalised tapered optical fiber is first immobilized with the 0.1 μM probe DNA for 1 hour and followed by rinsing three times using DI water and air-dried. After the probe DNA is covalently immobilized, several concentrations of target complementary DNA (0.2 nM, 0.4 nM, 0.6 nM, 0.8 nM and 1.0 nM) and 1.0 nM non-complementary DNA are incubated for 1 hour. The tapered optical fiber surface is rinsed three times with DI water after soaking in each concentration of target DNA and then air-dried. For each concentration, the testing is performed with a new tapered optical fiber. The transmission output spectra of immobilized probe DNA and hybridized target DNA are recorded via optical spectrum analyser (Yokogawa AQ6331).

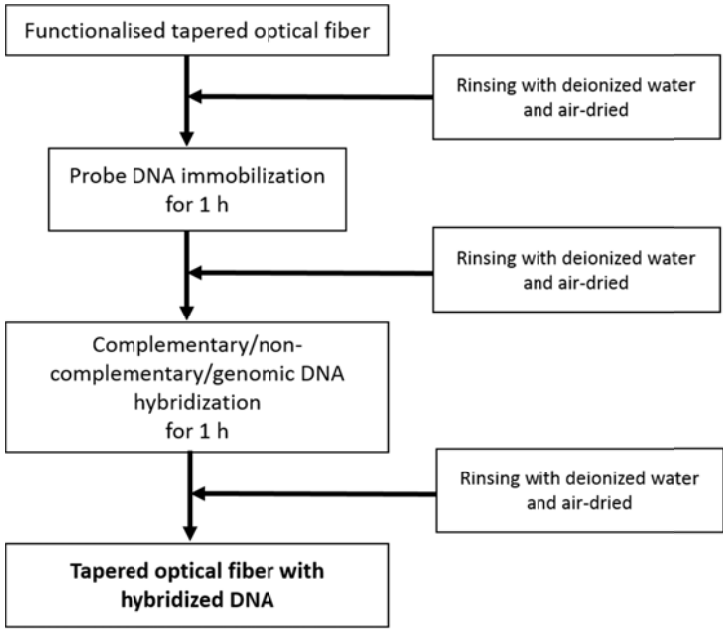

Figure 3 DNA immobilization and hybridization process.

Following that, genomic DNA from different bacteria were used in the cross-reactivity study. The genomic DNA tested were from the pathogenic *Leptospira interrogans* serovar Copenhageni and Canicola whereas the non-target control was *Clostridium difficile* (*C. difficile*) bacteria. The genomic DNA were acquired from Virology Laboratory, Universiti Putra Malaysia. The genomic DNA was thermally denatured at 95°C water for 2 minutes and rapidly cooled in ice water prior application to the system. This physical denaturation process was used by several previous studies[62, 63] to separate the double strand DNA into two single-stranded DNA and preserve the single-stranded prior use [64, 65].

2.4 Optical DNA detection system setup

The optical DNA detection system employed in the experiment is presented in Figure 4. The tapered optical fiber region is positioned within the straight groove of customized sensor holder. The immersion of analytes took place by carefully pipetting them to the vacant groove. Both ends of the tapered optical fiber are connected to the single mode FC/PC patch cords using the optical fiber fusion splicer machine (Sumitomo Electric Industries Ltd). The input end of the patch cord is fixed to the broadband light source (Amonics ALS 18-B-FA) with wavelength ranges from 1500 - 1600 nm while the output end is fixed to the optical spectrum analyser (OSA) (Yokogawa AQ6331). The OSA displays the transmission output spectrum which recorded by a customised LabView^{TM} program in the computer.

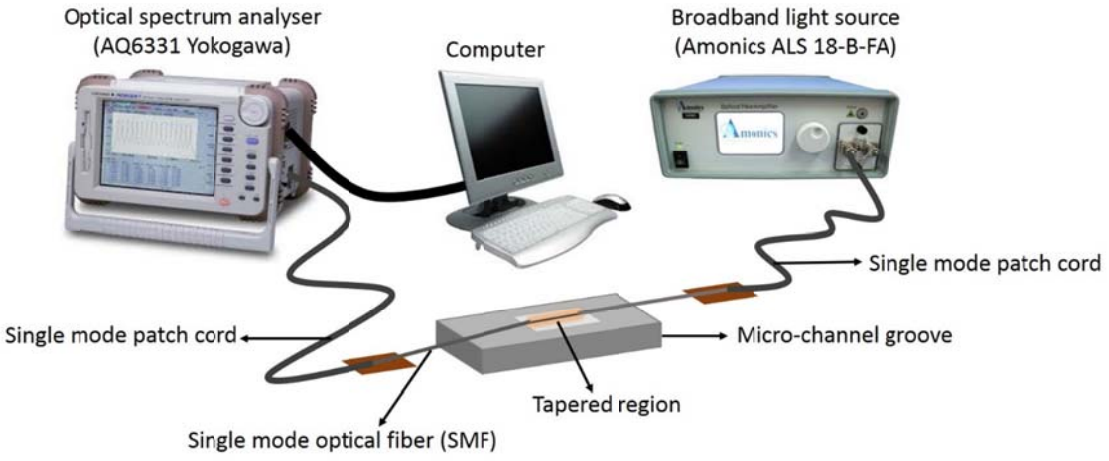

Figure 4 Experimental setup of the tapered optical fiber sensor.

2.5 Principle of optical biosensing in tapered fiber

In this work, optical biosensor is operated by utilizing the evanescent wave (EW) of propagated light in optical fiber as displayed in the schematic figure (Figure 5). The light propagates through optical fiber is owing to principle of total internal reflection where a core has higher refractive index than a cladding refractive index (n_{core}>n_{clad}). Under this condition, the standard single mode optical fiber (SMF) only allows the fundamental mode and its EW amplitude is exponentially decayed in the cladding.

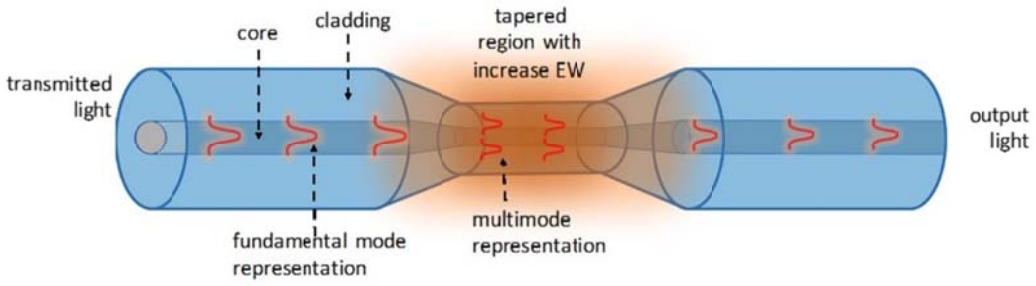

Figure 5 Schematic diagram of light propagation in tapered optical fiber.

The EW of the standard SMF is typically very low at core-cladding interface which almost no interaction with the external environment. Therefore, by tapering waist diameter of the SMF, the EW is extended beyond the normal core-cladding interface. As the light propagates through an air–cladding interface at the tapered region, the down-tapered region (as shown in Figure 1) allows the high-order mode. The tapered region is now converted into multimode fiber as it able to supports more than one mode. This is due to the large difference of the RIs of air and the silica (SiO_2) based optical fiber. The coupling of modes transmission occurs and then the EW portion increases at the tapered region [66]. This region is suitable for sensing purposes due to strong EW interaction with the surrounding.

The cladding interface at the tapered region is now transformed as a new core and the EW is enhanced on the new core-external medium interface. As a result, the interaction of the transmitted light with the surrounding medium is enhanced at the tapered region. The efficient interaction depends on the penetration depth (d_p) of evanescent wave and it is mathematically described as [67]:

$$d_p = \frac{\lambda}{2\pi(n_1^2 \sin^2\theta_{int} - n_{aq}^2)^{1/2}} \quad (1)$$

where λ is the wavelength of incident light, n_1 and n_{aq} are the RI of new core and external medium, and θ is the incident angle (°) measured from the normal at the interface of the new core and external medium.

Upon reaching up-tapered region, both fundamental and high-order modes begin to couple back together at the untapered region but with reduced intensity. As the fundamental and high-order modes are not in phase anymore, the result of back and forth coupling between the modes produce oscillations in the spectral response. The oscillations or periodic behaviour of the output spectrum is known as interferometric pattern (Mach-Zehnder interferometer) and can be observed via optical spectrum analyser (OSA) [68]. The output spectrum response of the tapered optical fiber can be explained in term of the output intensity expressed as [69]

$$I = I_1 + I_2 + 2\sqrt{I_1 I_2 \cos(\Delta\Phi)} \tag{2}$$

where I_1 and I_2 are the intensities of the fundamental and high-order modes, respectively, and ΔΦ is the phase shift between the two modes, which can be calculated using

$$\Delta\Phi = \left[\frac{2\pi(\Delta n_{eff})L_w}{\lambda}\right] \tag{3}$$

where n_{eff} is the difference between the effective refractive index of the core and the effective refractive index of the external surrounding ($n_c^{eff} - n_{ext}^{eff}$) and L_{w} is the waist length. The fringe spacing (ʌ) between two interference patterns is given by

$$\Lambda = \frac{\lambda^2}{\Delta n_{eff} L_w} \tag{4}$$

These equations mathematically support the idea that any manipulation of RI at the external surrounding or the cladding would affect the phase shift, fringe shift, as well as the resulting intensity of the output. Hence, when a sample of interest or a targeted analyte is introduced to the system, the occurrence of change in refractive index will be shown as the shifting of interference pattern between the spectra, as well as the difference in output intensity. The above equations mathematically promote the idea to characterize the tapered optical fiber by using different concentrations of NaCl. This is due to the fact that any manipulation of RI at the external surrounding would affect the phase shift, fringe shift, as well as the resulting

intensity of the output. The same concept is applied when a functionalised optical fiber is immobilized and hybridized with probe DNA and target DNA.

2.6 Principle of surface functionalisation of tapered optical fiber

The development of *Leptospira* DNA biosensor involves surface functionalisation process in order to graft the DNA biomolecules to the tapered optical fiber. The process exploits several chemical crosslinking reactions as anchoring point to attach the DNA. Refer to the scheme in Figure 6(a), the bare tapered optical fiber surface encounter hydroxylation process using NaOH solution. NaOH treatment introduces abundant surface hydroxyl groups (-OH) so that silanols on the fiber surface tend to form more hydrogen bond networks for further crosslinking reaction. The subsequent process is silanized the hydroxylated optical tapered fiber surface using APTES solution. Silanes are attached through the formation of a siloxane (Si-O-Si) bond between the surface and the silanol groups [70]. The bridged hydroxyl groups bonds with the Si-O-Si with free amine groups (-NH_2) as shown in Figure 6(b) and thereby, amine-modified optical fiber is produced. Ultimately, the amine-modified surface reacts with the glutaraldehyde (Figure 6(c)) to form a Schiff base linkage [71, 72]. Schiff base formation of both functional groups is significant to generate a stable and strong amino linkage for next crosslinking with biomolecules [73].

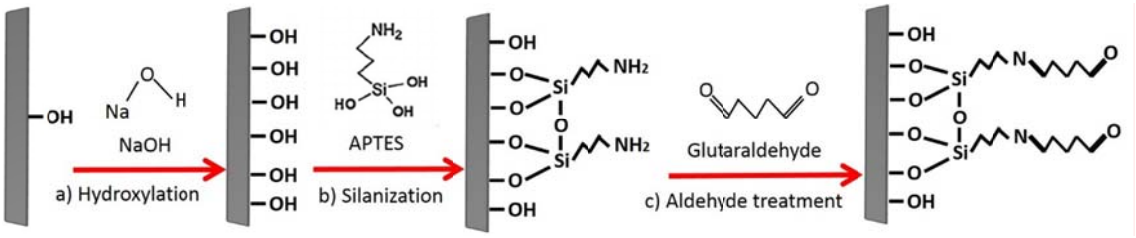

Figure 6 The process of a) hydroxylation by NaOH, b) silanization by APTES and c) crosslinking by glutaraldehyde on tapered optical fiber surface.

The hybridization of probe DNA and *Leptospira* DNA on the functionalised surface of the tapered optical fiber will result in the change of fiber surrounding refractive index. This will eventually be detected and measured as the shift of interference pattern between the spectra, as well as the difference in output intensity.

3. Result and discussions

3.1 Optical characterization and functionalisation of tapered optical fiber response

In this study, SMF diameter was abruptly reduced by heating a portion of the fiber while pulling its ends to generate the effects described in Section 2.5. The process changes the physical of optical fiber to a biconical transition regions and a relatively long waist region. The waist diameter can be modified about a few microns over a length of a few centimetres. Figure 7 displays a standard SMF with diameter of 125 µm (a) converted into the customised 12 µm tapered optical fiber (b). The figure clearly shows the transition of the standard SMF into the tapered SMF with down/up tapered length configuration stated in Figure 1.

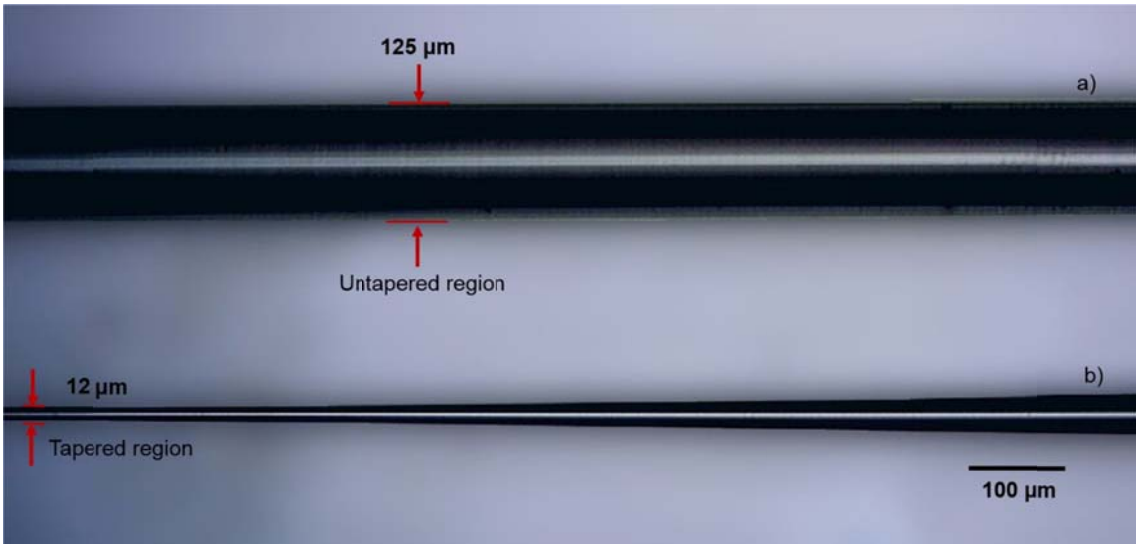

Figure 7 Microscopic image of a) untapered (standard) SMF and b) tapered optical fiber.

The tapered optical fiber is characterized by evaluating the responses of the tapered region towards different RI. Several concentrations of NaCl from 0.1 M to 0.5 M are used in order to induce the manipulation of RI. The spectrum is recorded when the tapered optical fiber region is fully immersed by NaCl solutions. All the spectra are then plotted in a graph as shown in Figure 8.

From the graph, the transmission spectra of the tapered optical fiber show the red shift and obvious interval of wavelength shift for each increasing concentration. This is due to the change of NaCl concentrations resulting in the change of RIs. The spectra support the theoretical expression of Eq. 4 to determine the red spectra shifts and larger fringe gap when the increases surrounding RI reduces the Δn_{eff}. Figure 9 illustrated the proportional wavelength shift ($\Delta\lambda$) of transmission spectra towards refractive index of NaCl. From that, a

good linear response is found with R^2 = 0.9776 while the sensitivity is achieved with 1905.7 nm/RIU which is comparable with previous study of same tapered profile dimension [45] within the same range of RI.

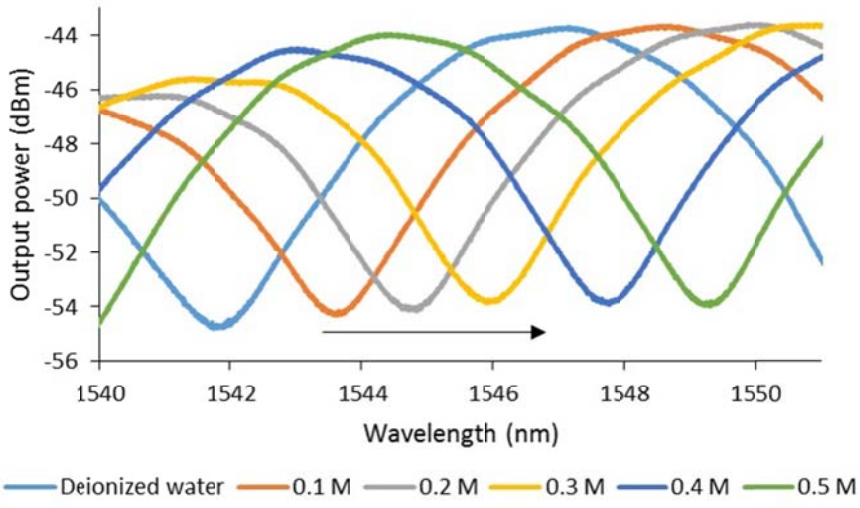

Figure 8 Transmission spectra of immersion NaCl into the tapered optical fiber region.

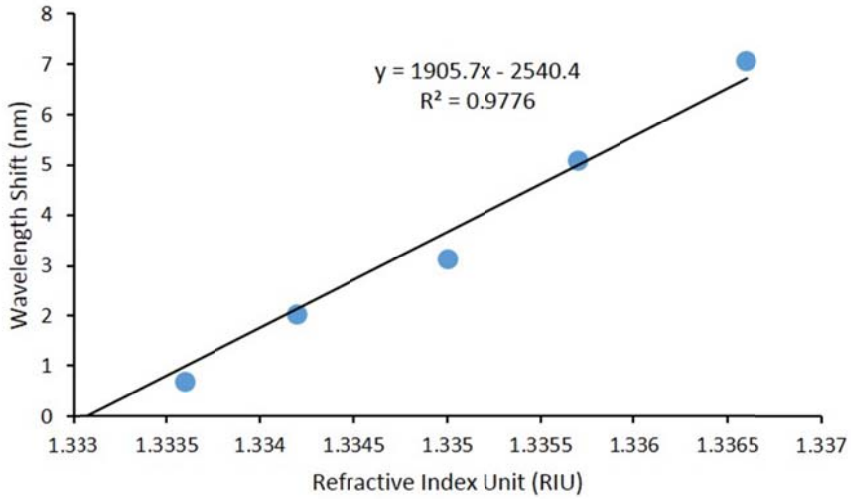

Figure 9 Relationship between wavelength shifts against refractive index of NaCl.

SEM is employed to observe the surface morphologies of untreated and each functionalised tapered optical fibers. The untreated bare optical fiber (Figure 10(a)) shows a smooth clean surface while the hydroxylating process by NaOH reveals there are some defects spotted on the tapered fiber surface (Figure 10(b)). The hydroxylation process by NaOH etches the tapered fiber and makes the surface coarser. The modified fiber surface is

suitable for the APTES attachment. The hydroxylated tapered optical fiber surface is fully covered with a rough coating after treatment with saline layer of APTES as shown in Figure 10(c). The figure indicates that the coating of APTES is homogeneously distributed around the tapered fiber surface. Subsequent reaction of aldehyde group with glutaraldehyde, the fiber surface texture becomes rougher as shown in Figure 10(c). Therefore, it can be seen that the surface modification is successfully carried out via these three chemical treatments.

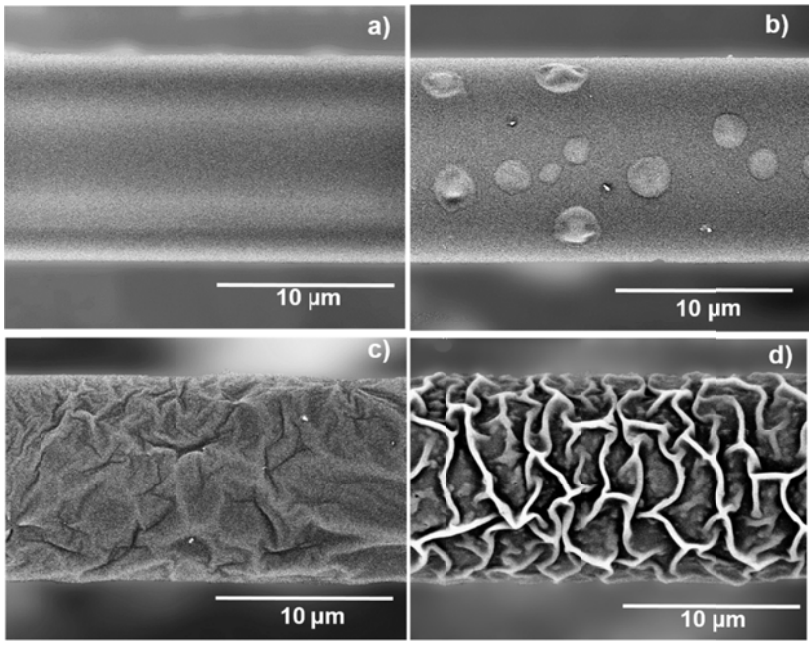

Figure 10 The surface morphology of a) bare tapered optical fiber, b) hydroxylated tapered optical fiber, c) amine-modified tapered optical fiber and d) aldehyde-modified.

Figure 11 demonstrates the transmission spectra of bare tapered optical fiber and the ones after NaOH hydroxylation, APTES silanization and glutaraldeyde treatment. All the transmission spectra shift to the red in response to each functionalisation reaction. Specifically, the interference dip response for NaOH hydroxylation shifts 0.83 nm to the right from adjacent dip response before treatment (bare fiber). Similar observations are perceived for other functionalisation as all their dip spectra shifts further to the right by 1.045 nm and 2.874 nm, respectively, for APTES and glutaraldehyde. Clearly, each of the functionalisation process has change the effective index of tapered optical fiber surface, thus verifying successful chemical bonding of the functional groups with the transducing platform.

The spectra in Figure 11 also show increment of 0.14 dB and 0.27 dB in transmission power after the tapered surface is treated with NaOH and APTES, respectively. Further and obvious increment 1.34 dB is observed after glutaraldehyde treatment. These trends might be

due to the phenomenon of light absorption occurred at the tapered optical fiber region. The light energies at the tapered region are absorbed by the molecules of coating layers (NaOH, APTES and glutaraldehyde) [74]. The light properties change at the tapered optical fiber causing the excited high order modes to shift its phase further from its initial phase and producing less efficient interferences when coupled back with the fundamental mode [75]. Therefore, this observation also justifies the success of the tapered optical fiber surface functionalisation.

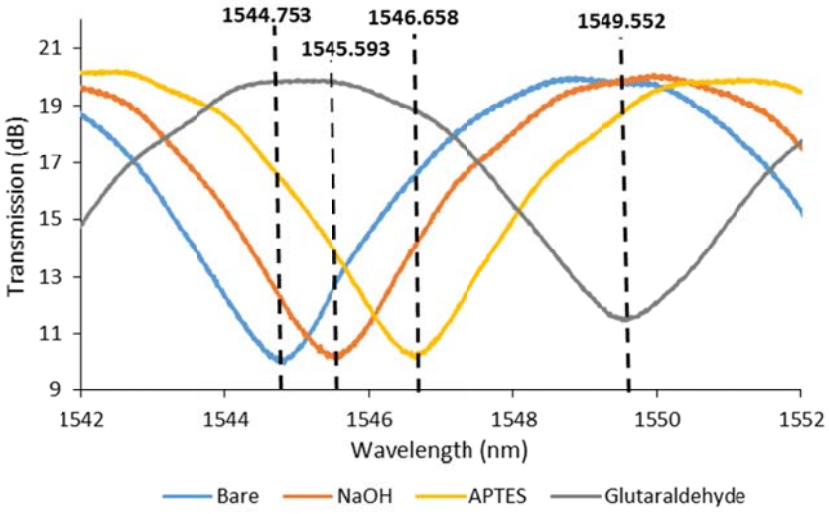

Figure 11 Transmission spectra of bare tapered fiber and NaOH, APTES and glutaraldehyde coated on the tapered fiber.

3.2 Immobilization of probe DNA and hybridization of complementary DNA response

After the tapered optical fiber is functionalised, it is then immobilized with probe DNA and hybridized with the complementary DNA. Immobilization occurred based on covalent bonding between aldehyde functional group on the tapered optical fiber with the probe DNA. Hybridization is the process of combining of two single stranded DNA (probe DNA and complementary DNA) into double stranded DNA [76]. When probe DNA with its complementary strand are aligned properly, hydrogen bonds form between the opposing complementary bases and the strands are joined [77].

The consequence of probe DNA binding with functionalised tapered optical fiber and complementary DNA binding with probe DNA leads to an increase in effective RI of the surface tapered fiber region. Such phenomenon established in Figure 12 revealed the red shift of transmission spectra response. The dip spectrum of immobilized probe DNA shifts

4.205 nm to the right from adjacent dip spectrum of glutaraldehyde coated fiber and its transmission power increase by 2.18 dB. Further dip spectrum shift of hybridized cDNA is observed and it shifts 1.97 nm to the right after probe DNA dip spectrum with further increasing transmission power of 0.83 dB. The shift of dip spectrum and changes of transmission parameter verifies modification of the tapered optical fiber surface by successful binding of targeted cDNA.

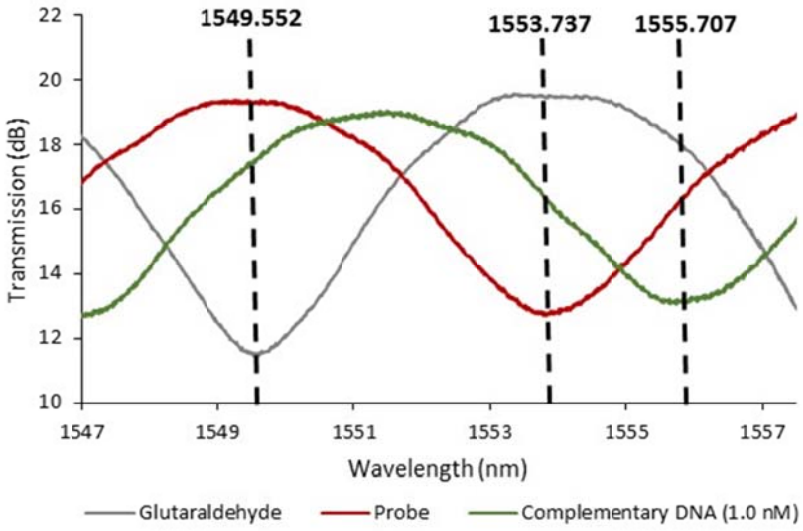

Figure 12 Spectra transmission of immobilization and hybridization of complementary DNA.

3.3 Sensitivity of tapered optical fiber towards complementary DNA

Dose-response graph of the wavelength shift versus DNA concentrations (in $\log_{10}$ scale) is presented in Figure 13 to indicate that the sensor is capable of working linearly in two ranges from 0.1 nM to 0.1 fM and 0.1 nM to 1 nM. However, 0.1 nM to 0.1 fM range produces smaller wavelength shift than the latter range (depicted in dotted lines in Figure 13). The effective sensing region is indicated by higher magnitude of wavelength shift, which is observed from 0.1 nM to 1 nM.

The sensitivity of this biosensor was determined based on its response to different concentrations of complementary DNA (0.1 nM to 1.0 nM) . The graph in Figure 14 exhibits good linearity of 0.9877 and sensitivity value of 1.2862 nm/nM which is better than previous DNA biosensors (0.27 nm/μM) [78]. This response is produced because at higher concentration of complementary DNA, there are more target complementary DNA bound to the probe DNA which consequently increases the effective RI of the surface. The sensor response is able to achieve wavelength shift from 0.705 nm for 0.1 nM (1E-10) to 1.945 nm

for 1 nM (1E-9) concentration (approximately 1.24 nm shift). This is stronger than the shift by Huang et al. (0.7 nm – 0.8 nm), and Gaos et al. (1 nm) for similar concentration range [40, 79]. Based on Figure 15, the developed sensor is able to detect concentrations as low as 0.1 fM which is more sensitive than several reported works using optical, electrochemical and colorimetric techniques [40, 61, 78–82].

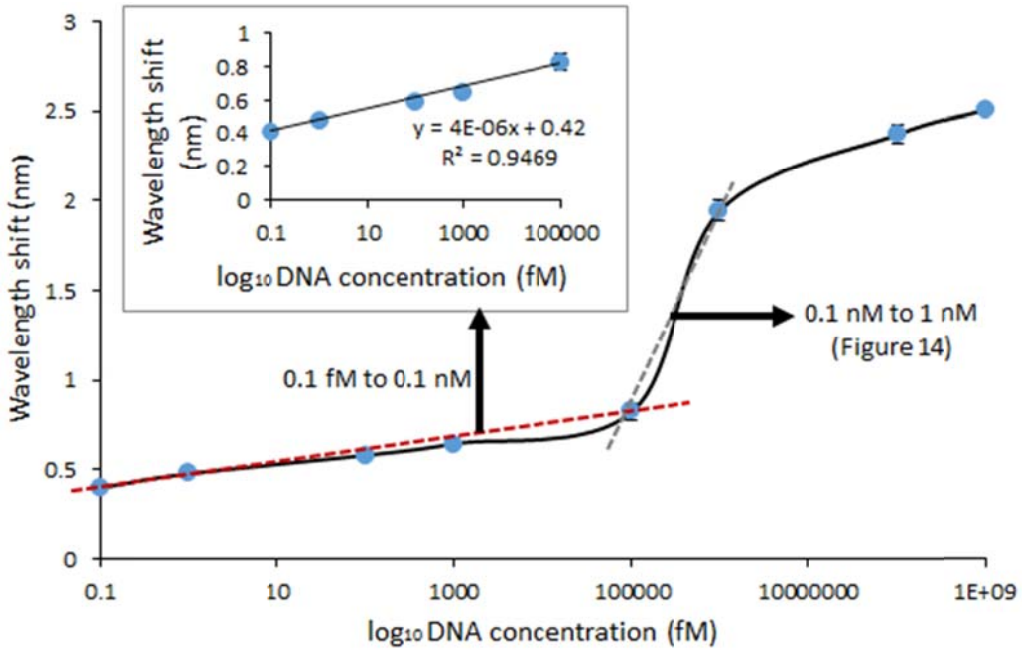

Figure 13 Dose-response graph of several DNA concentrations. Inset show the linear graph from 0.1 fM to 0.1 nM.

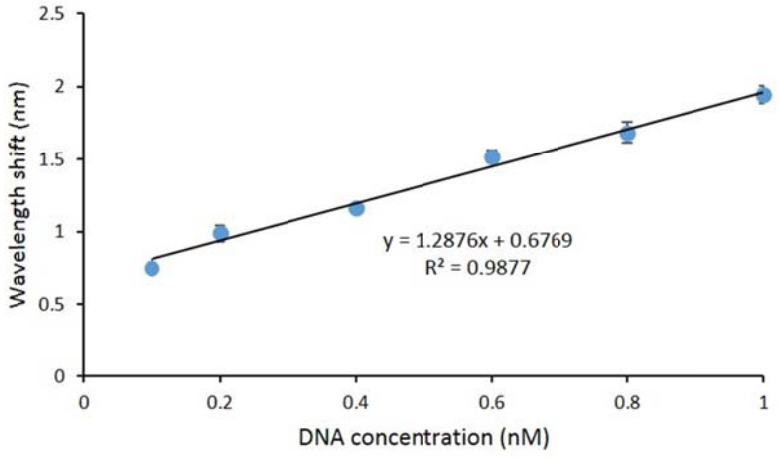

Figure 14 Relationship between wavelength shift and DNA concentrations.

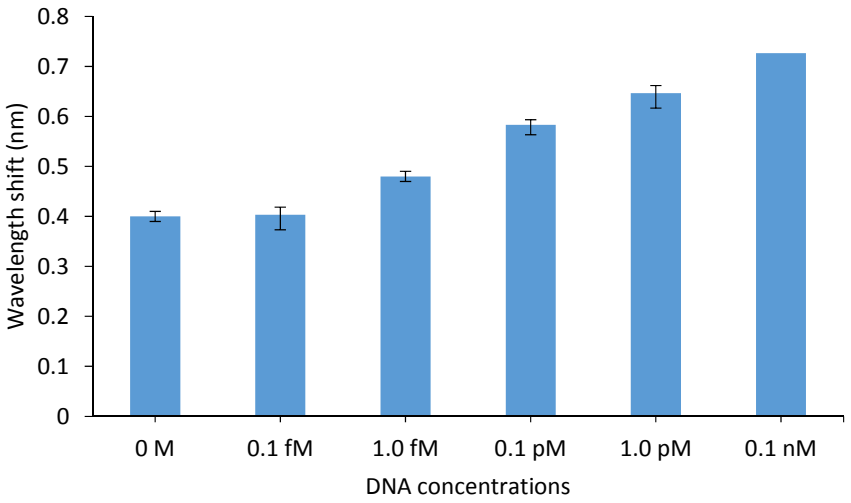

Figure 15 The wavelength shift of several DNA concentrations.

3.4 Sensor selectivity towards non-complementary DNA

Figure 16 illustrates the comparison result for wavelength shift of cDNA, non-complementary DNA and sterile ultrapure water after testing with the immobilized probe on tapered optical fiber sensor. Even though there is a slight shift when the sensor is tested with non-complementary DNA and sterile ultrapure water, the wavelength shift with complementary DNA is much stronger and produces a distinct response which indicates the high specificity of the proposed sensor.

In hybridization, hydrogen bonds are significant in determining the duplex formation of complementary base pairs [83]. The orientation of the bases must be just right for the interaction to take place [84]. However, the non-complementary DNA bases are not complementary in structure, thus, not all of these bonds can be simultaneously replaced by hydrogen bonds between the bases. In other words, duplex formation between non-complementary DNA and the probe DNA partially lacks specificity in terms of complementary Watson Crick (WC) base pairings [85].

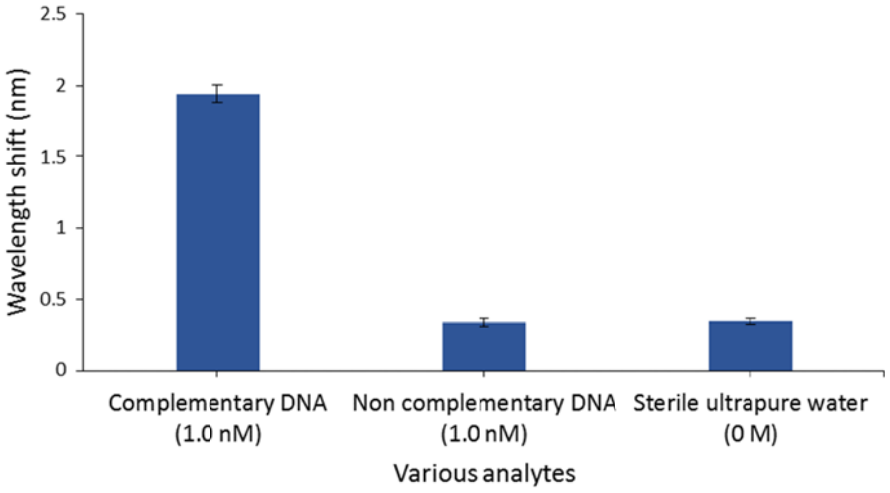

Figure 16: Histogram of the wavelength shift using different types of DNA in concentration of 1.0 nM

3.5 Sensor cross-reactivity study against genomic DNA sample

We then looked into the cross-reactivity study by observing the trait of wavelength shift towards various bacteria pathogens. *Leptospira interrogans* serovar Copenhageni and Canicola genomic DNA were used in this case to check for the feasibility of this system as a new insight in diagnosis of leptospirosis. Genomic DNA of *C. difficile* , a bacteria that infects the human intestine is used as a non-target control. As in Figure 17, a significant difference in wavelength shift is observed between the two *Leptospira* serovars against *C. difficile* when tested at concentration of 6.5 pg/µl for all samples, which indicates higher limit of detection (LOD) than the previous study by Wang et. al. with 1.7 ng/µl [86]. The wavelength shift achieved for Canicola and Copenhageni are 1.075 nm and 0.955 nm, respectively while the shift for *C. difficile* is recorded at 0.265 nm. The specificity is achieved as the probe DNA was particularly designed and aligned based on rrs gene of *Leptospira* spp.

The wavelength shift in Fig. 17 is much smaller than wavelength shift in Figure 16 even at equivalent concentration (1 nM corresponding to 6.5 pg/µL). The issue is related to the long DNA sequence of genomic DNA itself, which leads to the greater steric hindrance and lower adsorption of the target DNA [87]. The longer sequences of the DNA (more than 30 bases) also affect the efficiency of hybridization due to the agglutination of target molecule upon their binding on the sensing transducer [88]. Nevertheless, the outcome of this cross-reactivity testing shows the analogous performance with the works reported in [11] and [91], thus, verifying the sensor's adaptability to detect longer genomic DNA sequence in real

samples. From that, it can be concluded that the proposed tapered optical sensor is able to successfully detect and distinguish *Leptospira* DNA from other bacteria species.

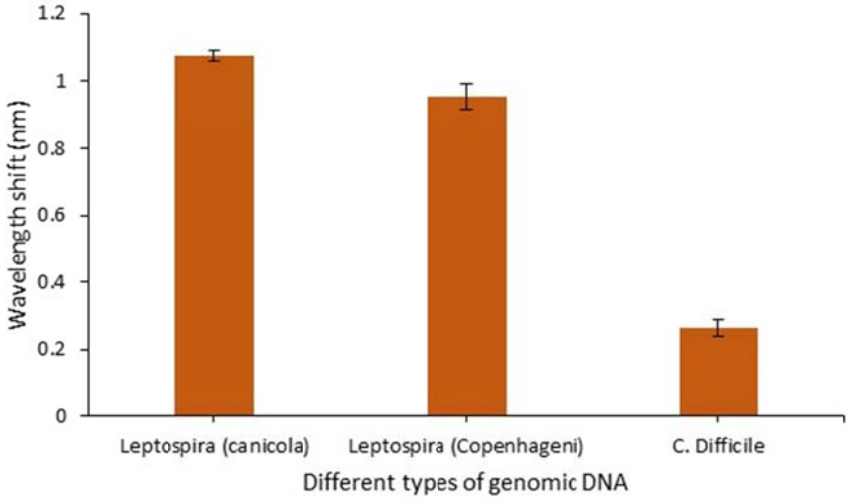

Figure 17 Histogram of the wavelength shift using different types of bacteria DNA in concentration of 6.5 pg/µl

4. Conclusion

In summary, we have successfully developed a tapered optical fiber sensor as a platform for *Leptospira* DNA detection. The characterization of tapered optical fiber is was accomplished by monitoring the transmission wavelength shift with sensitivity of 1905.7 nm/RI when tapered optical fiber is immersed in sodium chloride (NaCl). The wavelength shift was observed for each functionalisation step on the tapered region, immobilization of the probe DNA and hybridization of complementary DNA (cDNA). A linear wavelength shift response was obtained with increasing concentrations of the complementary DNA and the sensitivity achieved is 1.2862 nm/nM.

As for specificity, the sensor was able to selectively distinguish the presence of complementary DNA from non-complementary target DNA as well as *Leptospira* genomic DNA from the non-target bacteria. Both the genomic DNAs of *Leptospira* serovars Canicola and Copenhageni gave significant wavelength shifts compared to the non-target control bacteria (*C. difficile*). The strong optical biosensing performance of the tapered fiber also shows very good LOD (fM) and low target concentrations detection. On the other hand, there is a concern on the duration of the sensor probe functionalisation process which is

approximately 150 min. It is believed that the process can be significantly improved by implementing UV irradiation that takes only 10 min as reported by some studies [90-92]. Combining the UV irradiation method for quick probe functionalisation with the high sensitivity and specificity tapered fiber, the proposed optical sensor will be highly feasible for early and in-situ *Leptospira* DNA detection system.

Acknowledgements The authors would like to express their thanks to Ministry of Higher Education for supporting the work through FRGS/1/2016/TK04/UPM/02/4 and LRGS/UPM/700-2/1/LRGS/5526400 grants. We also like to acknowledge Diagnostic Molecular Lab, Biotechnology and Nanotechnology Centre, MARDI, Serdang for allowing us to use the facilities for sample preparation. We are thankful to Lam Jia Yong for reading and correcting part of the manuscript and Shuhaidah Othman for preparing the *Leptospira* DNA.

References

1. A. I. Ko, C. Goarant, and M. Picardeau, Nat. Rev. Microbiol. **7**(10), 736–747 (2009).
2. D. A. Haake and P.N Levett, in *Leptospira and Leptospirosis*, Vol. 387, edited by B. Adler (Springer, Berlin, Heidelberg, 2015).
3. B. Abela-Ridder, R. Sikkema, and R. A. Hartskeerl, Int. J. Antimicrob. Agents, **36**, S5–S7 (2010).
4. B. Adler and A. de la Peña Moctezuma, Vet. Microbiol. **140**(3-4), 287–296 (2010).
5. S. Thayaparan, I. D. Robertson, A. Fairuz, L. Suut, and M. T. Abdullah, Malays. J. Pathol. **35**(2), 123–132 (2013).
6. C. H. Chang, M. Riazi, M. H. Yunus, S. Osman, and R. Noordin, Diagn. Microbiol. Infect. Dis. **80**(4), 278–281 (2014).
7. I. Shah, Pediatric Infectious Disease **4**(1), 4–8 (2012).
8. S. V. Budihal and K. Perwez, J. Clin. Diagn. Res. **8**(1), 199-202 (2014).
9. M. Picardeau, E. Bertherat, M. Jancloes, A. N. Skouloudis, K. Durski, and R. A. Hartskeerl, Diagn. Microbiol. Infect. Dis. **78**, 1–8 (2014).
10. F. R. R. Teles and L. P. Fonseca, Talanta **77**, 606–623 (2008).
11. M. Barozzi, A. Manicardi, A. Vannucci, A. Candiani, M. Sozzi, M. Konstantaki, S. Pissadakis, R. Corradini, S. Selleri, and A. Cucinotta, J. Lightwave Technol. **35**(16), 3461–3472 (2017).
12. Y. Yan, S. Ding, D. Zhao, R. Yuan, Y. Zhang, and W. Cheng, Sci. Rep. **6**, 1–9 (2016).
13. J. T. Gerig, *Introductory Organic Chemistry* (Elsevier, 2012).

14. K.l Skold, M. Svensson, G. Palmers, and P. E. Andrén (United States Patent), US8663959B2, **2014**.
15. C. Cenciarini-borde, S. Courtois, and B. La Scola, Future Microbiol. **4**(1), 45-64 (2009).
16. Z. Lewandowski and H. Beyenal, *Fundamentals of Biofilm Research* (CRC Press, Boca Raton, 2014).
17. G. Wandemur, D. Rodrigues, R. Allil, V. Queiroz, R. Peixoto, M. Werneck, and M. Miguel, Biosens. Bioelectron. **54**, 661–666 (2014).
18. Z. Jennifer Guo, C. Boyter, G. Cohoon, E. Salik, and W. Lin, GSTF Journal on Bioinformatics and Biotechnology **1**(1), 36–42 (2011).
19. Chen Liu, C. Liu, M. D. Hughes, D. A. Nagel, A. V Hine, and L. Zhang, J. Biosens Bioelectron. **6**(2), 2015.
20. Z. B. Bahşi, A. Büyükaksoy, S. M. Ölmezcan, F. Şimşek, M. H. Aslan, and A. Y. Oral, Sensors **9**(6), 4890–4900 (2009).
21. T. A. Birks, B. J. Mangan, A. Díez, J. L. Cruz, and D. F. Murphy, Opt. Express **20**(13), 13996-14008 (2012).
22. H. Latifi, M. I. Zibaii, S. M. Hosseini, and P. Jorge, Photonic Sens. **2**(4), 340–356 (2012).
23. M. Pospíšilová, G. Kuncová, and J. Trögl, Sensors **15**(10), 25208–25259 (2015).
24. G. Y. Chen, M. Ding, T. P. Newson and G. Brambilla, Open Opt. J. **7**, 32-57 (2013).
25. P. Wang, G. Brambilla, M. Ding, T. Lee, L. Bo, Y. Semenova, Q. Wu, and G. Farrell, IEEE Sens. J. **13**(1), 180–185 (2013).
26. S. Mas, J. Martí, D. Monzón-Hernández, and J. Palací, Opt. Commun. **361**, 99–103 (2016).
27. J. Kou, J. Feng, Q. Wang, F. Xu, and Y. Lu, Opt. Lett. **35**(13), 2308-2310 (2010).
28. J. Wo, G. Wang, Y. Cui, Q. Sun, R. Liang, P. P. Shum, and D. Liu., Opt. Lett. **37**(1), 67-69 (2012).
29. P. Lu, J. Harris, X. Wang, G. Lin, L. Chen, and X. Bao, Appl. Opt. **51**(30), 7368–7373 (2012).
30. J. Musayev, Y. Adlgüzel, H. Külah, S. Eminoglu, and T. Akln, IEEE Sens. J. **14**(5), 1608–1616 (2014).
31. M. R. K. Soltanian, A. S. Sharbirin, M. M. Ariannejad, I. S. Amiri, R. M. De La Rue, G. Brambilla, B. M. A. Rahman, K. T. V. Grattan, and H. Ahmad IEEE Sens. J. **16**(15), 5987– 5992 (2016).

32. H. S. Haddock, P. M. Shankar, and R. Mutharasan, Sens. Actuators, B **88**(1), 67–74 (2003).
33. Y. Tian, W. Wang, N. Wu, X. Zou, and X. Wang, Sensors **11**(4), 3780–3790 (2011).
34. G. J. Wang and Z. Bin Wang, Appl. Mech. Mater. **687–691**, 3403–3406 (2014).
35. S. C. Warren-Smith and T. M. Monro, Opt. Express **22**(2), 1480-1489 (2014).
36. Y. Liu, C. Meng, A. P. Zhang, Y. Xiao, H. Yu, and L. Tong, Opt. Lett. **36**(16), 3115 3117 (2011).
37. T. K. Yadav, R. Narayanaswamy, M. H. Abu Bakar, Y. M. Kamil, and M. A. Mahdi, Opt. Express **22**(19), 22802- 22807 (2014).
38. D. Liu, A. K. Mallik, J. Yuan, C. Yu, G. Farrel, Y. Semenova, and Q. Wu, Opt. Lett. **40**(17) 4166–4169 (2015).
39. A. Candiani, M. Sozzi, A. Cucinotta, S. Selleri, R. Veneziano, R. Corradini, R. Marchelli, P.Childs, and S. Pissadakis, IEEE J. Sel. Top. Quantum Electron. **18**(3), 1176–1183 (2012).
40. Y. Huang, B. Yu, T. Guo, and B. Guan, RSC Adv. **7**(22), 13177–13183 (2017).
41. S. Pilevar, C. C. Davis, and F. Portugal, Anal. Chem. **70**(10), 2031–2037 (1998).
42. Y. Mustapha Kamil, M. H. Abu Bakar, M. A. Mustapa, M. H. Yaacob, N.H.Z. Abidin, A. Syahir, H.J. Lee, and M.A. Mahdi, Sens. Actuators, B **257**, 820-828 (2008).
43. T. Reynolds, M. R. Henderson, A. François, N. Riesen, J. M. M. Hall, S. V. Afshar, S. J. Nicholls, and T. M. Monro, Opt. Express **23**(13), 17067–17076 (2015).
44. A. François, N. Riesen, H. Ji, S. Afshar V., and T. M. Monro, Appl. Phys. Lett. **106**(3), 31104 (2015).
45. Y. Mustapha Kamil, M. H. Abu Bakar, M. A. Mustapa, M. H. Yaacob, A. Syahir, and M. A. Mahdi, IEEE Photonics J. **7**(6), 3700109 (2015).
46. M. D. Sonawane and S. B. Nimse, Journal of Chemistry **2016**, 1-19 (2016).
47. Y. Maruyama, S. Terao, and K. Sawada, Biosens. Bioelectron. **24**(10), 3108–3112 (2009).
48. E. Özkumur, S. Ahn, A. Yalcın, C. A. Lopez, E. Cevik, R. J. Irani, C. DeLisi, M. Chiari, and M. Selim Ünlü, Biosens. Bioelectron. **25**(7), 1789–1795 (2010).
49. Q. Wang, B. Zhang, X. Lin, and W. Weng, Sens. Actuators, B **156**(2), 599–605 (2011).
50. Z. Qiang, L. Junyang, Y. Yanling, G. Libo, and X. Chenyang, Optik **125**, 4614–4617 (2014).
51. D. Sun, Y. Ran and G. Wang, Sensors **17**(2559), 1-8 (2017).

52. S. Pal, M. J. Kim, and J. M. Song, Lab Chip **8**, 1332–1341 (2008).
53. Z. Zhang, F. Hua, T. Liu, Y. Zhao, J. Li, R. Yang, C. Yang, and L. Zhou. PLoS One **9**(5), 1-8 (2014).
54. A. J. S. Ribeiro, K. Zaleta-rivera, E. A. Ashley, and B. L. Pruitt, ACS Appl. Mater. Interfaces **6**, 15516-15526 (2014).
55. H. H. Lin, I. Wang, P. Yen, H. Cheng, H. Tsai, H. Liao, S. Lu, F. Chou, and C. Lin, Procedia Eng. **87**, 340–343 (2014).
56. W. Lai, C. Lin, Y. Yang, and M. S. C. Lu, Biosens. Bioelectron. **35**(1), 456–460 (2012).
57. M. Chuang, C. Liu, and M. Yang, Sens. Actuators, B **114**(1), 357–363 (2006).
58. P. Sonthayanon, W. Chierakul, V. Wuthiekanun, J. Thaipadungpanit, T. Kalambaheti, S. Boonsilp, P. Amornchai, L. D. Smythe, D. Limmathurotsakul, N. P. Day, and S. J. Peacock, Am. J. Trop. Med. Hyg. **84**(4), 614–620 (2011).
59. M. Kaisti, A. Kerko, E. Aarikka, P. Saviranta, Z. Boeva, T. Soukka and A. Lehmusvuori, Sci. Rep. **7**(1) 1–8 (2017).
60. A. Karimizefreh, P. Sasanpour, E. Jokar, R. Mohammadpour, M. Vaezjalali, and T. Tekieh, IEEE Int. Sci. Conf. Electron. Nanotechnol. **34**, 368–370 (2014).
61. N. Oliveira, E. Souza, D. Ferreira, D. Zanforlin, W. Bezerra, M. Amélia Borb, M. Arruda, K. Lopes, G. Nascimento, D. Martins, M. Cordeiro and J. Lima-Filho, Sensors **15**(7), 15562–15577 (2015).
62. X. Wang, H. J. Lim, and A. Son, Environmental Health and Toxicology **29**, 1-8 (2014).
63. D. S. Campos-Ferreira, E. V.M. Souza, G. A. Nascimento, D. M.L. Zanforlin, M. S. Arruda, M. F.S. Beltrao, A. L. Melo, D. Bruneska, J. L. Lima-Filho, Arabian J. Chem. **9**(3), 443–450 (2016).
64. C. Ignac, *DNA Engineered Noble Metal Nanoparticles* (Wiley-Scrivener, USA, 2015).
65. Richard Sinden, *DNA Structure and Function* (Elsevier, 2012).
66. T. Martan, J. Kanka, I. Kasik, and V. Matejec, International Journal of Optomechatronics **3**(3), 233–249 (2009).
67. M. Ahmad and L. L. Hench, Biosens. Bioelectron. **20**(7), 1312–1319 (2005).
68. M. I. Zibaii, H. Latifi, M. Karami, M. Gholami, S. M. Hosseini, and M. H. Ghezelayagh, Meas. Sci. Technol. **21**(10), 1-12 (2010).
69. T. K. Yadav, M. A. Mustapa, M. H. Abu Bakar, and M. A. Mahdi, J. Europ. Opt. Soc. Rap. Public. **9**, (2014).
70. R. M. Pasternack, S. R. Amy, and Y. J. Chabal, Langmuir **24**(9), 12963–12971 (2008).

71. I. Migneault, C. Dartiguenave, M. J. Bertrand, and K. C. Waldron, BioTechniques **37**(5), 790–802 (2004).
72. X. Liu, Z. Ma, J. Xing, and H. Liu, J. Magn. Magn. Mater. **270**, 1-6 (2004).
73. S. Wickramaratne, S. Mukherjee, P. W. Villalta, O. D. Scharer and N. Y. Tretyakova, Bioconjugate Chem. **24**, 1496-1506 (2013).
74. A. Urrutia, J. Goicoechea, and F. J. Arregui, Journal of Sensors **2015**, 1-18 (2015).
75. C. Lee, W.Shih, J. Hsu, and J. Horng, Opt. Express **22**(20), 24646–24654 (2014).
76. S. Sudheer, *Doctor of Philosophy*, Duke University(North Carolina, USA), **2007**.
77. S. C. Presnell, in *The Molecular Basis of Human Cancer*, edited by W. B. Coleman and G. J. Tsongalis (Springer Science+Business Media, New York, 2002, Ch. 2).
78. M. Yin, C. Wu, L. Shao, W. K. E. Chan, A. P. Zhang, C. Lu, and H. Tam, Analyst **138**, 1988–1994 (2013).
79. S. Gao, L. Sun, J. Li, L. Jin, Y. Ran, Y. Huang, and B. Guan, Opt. Express *25*(11),13305–13312 (2017).
80. Y. Huang, Z. Tian, L. Sun, D. Sun, J. Li, Y. Ran, and B. Guan, Opt. Express **23**(21), 26962–26968 (2015).
81. D. Sun, T. Guo, Y. Ran, Y. Huang, and B. Guan, Biosens. Bioelectron. **61**, 541–546 (2014).
82. J. Thavanathan, N. M. Huang, and K. L. Thong, Biosens. Bioelectron. **55**, 91–98 (2014).
83. H. S. Stoker, *Organic and Biological Chemistry*, (Cengage Learning, 2011).
84. T. Tian, Z. M. LeJeune, W. K. Serem, J. Yu, and J. C. Garno, in *Tip-Based Nanofabrication*, edited by A. A. Tseng, (Springer Science+Business Media, New York, 2011).
85. B. Schneider and H. M. Berman, in *Computational studies of RNA and DNA*. Edited by J. Šponer, and F. Lankaš, (Springer, Netherlands, 2006).
86. X. Wang, K. L. Cooper, A. Wang, J. Xu, Z. Wang, Y. Zhang, and Z. T. Virginia, Appl. Phys. Lett. **89**(163901), (2006).
87. X. Yang, K. Yang, X. Zhao, Z. Lin, Z. Liu, S. Luo, Y. Zhang, Y. Wang, and W. Fu, Analyst **142**(24), 4661-4669 (2017).
88. W. J. Parak, T. Pellegrino, C. M. Micheel, D. Gerion, S. C. Williams, and A. P. Alivisatos, Nano Lett. **3**(1), 33–36 (2003).
89. X. Liu and W. Tan, Anal. Chem. **71**(22), 5054–5059 (1999).

90. A. J. Haes, L. Chang, W. L. Klein, and R. P. Van Duyne, J. Am. Chem. Soc. **127**(7), 2264–2271 (2005).
91. R. Peltomaa, S. Vaghini, B. Patiño, E. Benito-Peña, and M. C. Moreno-Bondi, Anal. Chim. Acta **935**, 231–238 (2016).
92. J. Escorihuela, M. J. Bañuls, R. Puchades, and Á. Maquieira, Bioconjugate Chem. **23**(10), 2121–2128 (2012).